Anisotropic compression effects on nanocrystalline crystals of nickel oxide

Masaki Mito[1],* Takayuki Tajiri[2],† Seiya Saisho[1], Hiroyuki
Deguchi[1], Atsushi Kohno[2], and Kazuma Nakamura[1]

[1] *Faculty of Engineering, Kyushu Institute of Technology, Kitakyushu 804-8550, Japan and*

[2] *Faculty of Science, Fukuoka University, Fukuoka 814-0180, Japan*

(Dated: May 11, 2019)

Abstract

Nickel oxide (NiO) with bulk crystalline size is an antiferromagnetic insulator correlated strongly with crystal structure. A reduction in crystalline size causes a change in the magnetic sublattice, resulting in the appearance of ferromagnetic moments. Furthermore, in the nano crystals fabricated in mesoporous silica, there is a lattice distortion at the unit cell level that brings about the change in the magnetic property, suggesting a prominent magneto-structural correlation. We investigate anisotropic compression effects on nanocrystalline NiO with a crystalline size (D) of 11.4 nm to observe this remarkable magneto-structural correlation. Magneto-crystalline anisotropy is at its maximum when negative contraction occurs. The negative contraction appears even in a bulk crystal under non-ideal hydrostatic compression, and its anomalous structural change is suppressed with decreasing D.

---

*Electronic address: `mitoh@mns.kyutech.ac.jp`

†Electronic address: `tajiri@fukuoka-u.ac.jp`

1

I. INTRODUCTION

The history of nickel oxide (NiO) is long in both theoretical and experimental studies. In 1958, Roth studied the magnetic structure of NiO together with transition metal oxides, such as MnO, FeO, and CoO [1]. In 1964, Rodbell and Owen reported sublattice magnetization and lattice distortions in MnO and NiO [2]: The cubic structure of NiO changes to a rhombohedral structure below the Néel temperature T_N (=523 K) as shown in Fig. 1. The temperature dependence of unit cell volume for the family material MnO has been confirmed to exhibit rapid change at T_N (~120 K) [3]. In 1984, this strong magneto-structural correlation in NiO was actively discussed from the viewpoint of either the band insulator or the Mott insulator through theoretical studies [4–6] and photoemission measurements [7, 8]. Since then, there have been many theoretical studies, such as supercell local-density calculation in 1986 [9], spin-polarized band-structure calculation in 1990 [9], Ab inito study in 1994 [10] and 2000 [11], and quasiparticle band structure in 2009 [12]. Given this background, when spin polarization is not considered, the electronic state becomes metallic. The spin polarization stabilizes the insulating state, indicating that the electronic state is strongly coupled with antiferromagnetic magnetic ordering.

The effects of the aforementioned strong magneto-electro-structural correlation appear more prominently in nano-size systems: The magnetic sublattice changes from a two-sublattice structure to an eight-sublattice one, resulting in the appearance of ferromagnetic moments [13, 14]. Some of us investigated the magneto-structural correlation in NiO nanocrystals synthesized in mesoporous silica [15]: At approximately 3 nm, the rhombohedral structure of the nanocrystals is severely strained, and both the elongation of the unit cell along the [111] direction and the unit cell volume are at their maximum values. The nanocrystals with the above critical size exhibit the largest magnetic anisotropy, accompanying magnetic hysteresis and magnetic dynamics with energy loss. Thus, for large surface ratios, the magneto-structural correlation effect is further stimulated.

We imagine that, if the structural modification is performed on nano-sized NiO, remarkable changes in both crystal structure and magnetic properties would be expected. The experimental knowledge observed should be valuable for understanding the magneto-structural correlation of NiO in more detail. The detailed strategy of the present study is to conduct the structural manipulation artificially for nanocrystalline NiO with the mean
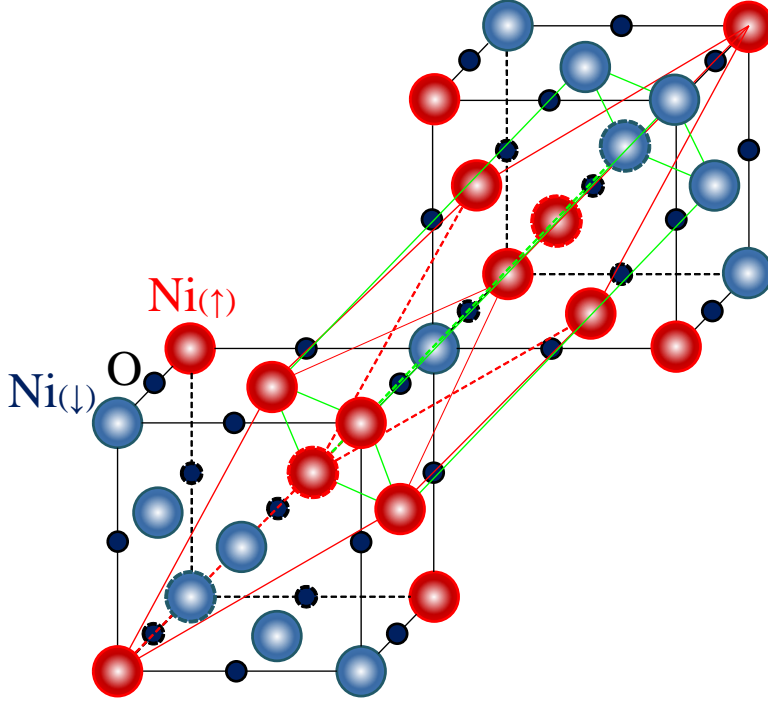
FIG. 1: Crystal structure of NiO, displayed in both manners of face-centered cubic (fcc) and rhombohedral unit cells to present two kinds of layers stacking along the [111] direction of the fcc lattice. Considering the antiferromagnetic spin structure, we should adopt the rhombohedral unit cells displayed with red lines. For the sake of comparing our results with previous studies, however, the hexagonal unit cell based on the rhombohedral system is displayed with green lines, and the ratio of lattice constants, c/a, presents the elongation along the [111] direction of the fcc lattice.

crystalline size D of 11.4 nm, embedded in mesoporous silica with a pore diameter size of approximately 7 nm, by the use of non-hydrostatic compression (*i.e.* "anisotropic compression permitting Poisson effect intrinsically"). The magneto-structural correlation is then discussed. Further, the artificial structural change is also investigated for nanocrystalline NiO with $D = 8.6$, 17.1, and 24.6 nm. The unique structural change under anisotropic compression (Fig. 2(c)) observed is discussed through comparison with the bulk system under "isotropic compression" (Fig. 2(a)) and "anisotropic compression" Fig. 2(b)).

For reference, there is a previous study on the effects of "anisotropic compression permitting Poisson effect intrinsically" on perovskite $LaMnO_{3+\delta}$ nanocrystals, with a crystalline size of 10 nm and rhombohedral symmetry, embedded in mesoporous silica [16].

Finally, the presented results for nanocrystalline NiO are compared with previous results for nanocrystalline LaMnO$_{3+\delta}$ to demonstrate the characteristic magneto-structural correlation in nanocrystalline NiO. In addition, an anomalous phenomenon induced by strain-accumulation, observed in NiO, is compared with a recent study on a severely strained superconductor Nb [17].
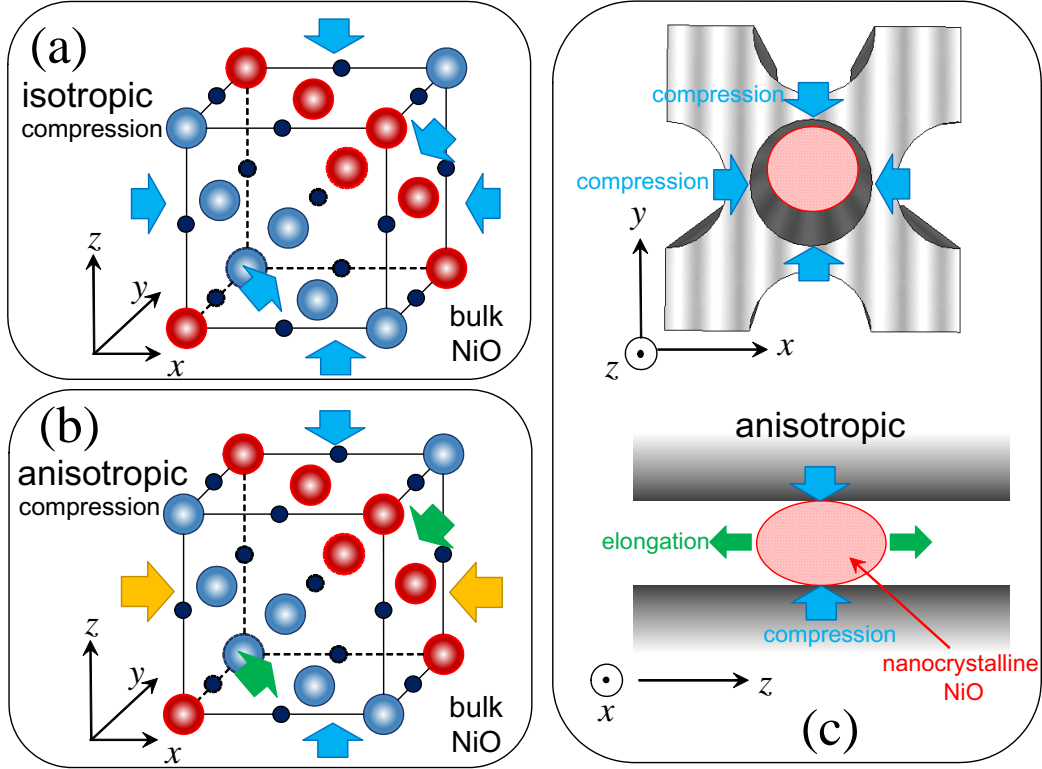

FIG. 2: (Color online) Compression style in bulk (a, b) and nanocrystalline (c) NiO crystals: (a) Isotropic compression for bulk crystal realized by ideal hydrostatic compression (ideal case realized by the DFT calculation), (b) anisotropic compression for bulk crystal realized by quasi-hydrostatic compression (realistic case realized in the high-pressure experiment using a certain pressure-transmitting medium (PTM)), (c) anisotropic compression permitting Poisson effect intrinsically for nanocrystalline crystal synthesized in mesoporous silica (realized in the high-pressure experiment using a certain PTM). The nanoparticles in the one-dimensional pores were crushed in the direction parallel to the silica walls. Given a rectangular coordinate system, there are two manners, such as compression along two directions and elongation along a residual direction.

4

II. EXPERIMENTAL PROCEDURE AND CALCULATION

NiO nanocrystals were synthesized according to the procedure described elsewhere [15]. The NiO nanoparticles were synthesized in one-dimensional pores of mesoporous silica SBA-15, which has a well-ordered two-dimensional hexagonal mesoporous structure. In the present study, we used SBA-15 with a pore diameter of approximately 7 nm as a template to equalize particle size during the fabrication of NiO nanoparticles. NiO powder was synthesized from the precursor solution for fabrication of NiO nanoparticles, which was an aqueous solution of $(CH_3COO)_2Ni \cdot 4H_2O$. The powder obtained by drying the aqueous solution was calcinated in an air atmosphere at $650°C$. The average crystallite size was estimated based on the peak positions and the full width at half maximum of the Bragg peaks using Scherrer's equation. It has been confirmed through the powder X-ray diffraction (XRD) and transmission electron microscope (TEM) experiments that the average crystallite size for nanocrystals is nearly consistent with the crystalline size D [15]. Their physical properties at ambient pressure have already been reported elsewhere [15].

The AC magnetic susceptibility was observed using a superconducting quantum interference device (SQUID) magnetometer equipped with an AC option. The amplitude of the AC field was 3.9 Oe and the frequency covered 1 to 100 Hz. Furthermore, the magnetization (M) curve was measured at $T = 5$ K, and the coercive field H_c was evaluated. High pressure was attained using a piston cylinder cell made of CuBe [18]. Apiezon-J oil, as a pressure-transmitting medium (PTM), was mixed with the sample (18.0 mg for the mixture of NiO and SBA-15), and the pressure value was evaluated according to the calibration data between the load value and low-temperature pressure estimated from the superconducting transition temperature of lead [18]. Herein the pressure value estimated here corresponds to the magnitude of pressure which SBA-15 receives.

XRD analysis was conducted under hydrostatic compression of up to approximately 30 kbar (= 3 GPa) at room temperature using a synchrotron radiation XRD system with a cylindrical imaging plate at the Photon Factory (PF) at the Institute of Materials Structure Science, High Energy Accelerator Research Organization (KEK) [19]. The wavelength of the incident X-rays in the pressure experiment was 0.88444 Å. Pressure was applied using a diamond-anvil cell, which consisted of two diamond anvils with flat tips having a diameter of 0.8 mm and a 0.3 mm-thick CuBe gasket. The bulk NiO powders, passed through a sieve

with an aperture of 20 μm or a mesoporous silica SBA-15 containing the NiO nanocrystals, were contained in a sample cavity with a diameter of 0.4 mm, along with a ruby used as a manometer and fluorinated oil (Sumitomo 3M Ltd., FC-77) or a 4:1 mixture of methanol and ethanol as PTM. The magnitude of pressure (P) was estimated by measuring the fluorescence of the ruby [20]. The structural parameters were estimated by Rietveld analysis [21]. The experiment was performed at a room temperature lower than T_{c} (=523 K). According to the previous studies for bulk NiO [2] and nanocrystalline NiO [15], the XRD pattern at room temperature is analyzed with the rhombohedral system.

Spin density functional calculations with plane-wave basis sets were performed using the xTAPP code [22], where the ultrasoft pseudopotential [23, 24] and the generalized gradient approximation of the exchange correlation potential were employed [25]. The cutoff energies in the wavefunction and charge densities were 169 and 676 Ry, respectively, and the atomic and cell parameters with given external pressure were optimized with a 6×6×6 k-point sampling. The spin ordering is assumed to be type-II antiferromagnetic, and the unit cell contains four atoms (two nickel and oxygen atoms). In the cell optimization with constant cutoff energy, electronic kinetic energies were corrected to not generate artificial discontinuity of the total energy due to the different basis set size [26]. We note that highly accurate convergence of stress within 10^{-5} (atomic units per atom) is needed to obtain correct cell parameters with given external pressure.

In this study, we target the pressure scale of the pressure experiment as approximately below 2 GPa. Thereby, we use kbar as the unit of pressure instead of GPa to keep a valid number of the pressure value.

III.   EXPERIMENTAL RESULTS OF NANO-SIZED NIO

A.   Magnetic measurement

Figure 3(a) shows the temperature dependence of the out-of phase of AC magnetic susceptibility χ" of nanocrystalline NiO with $D = 11.4$ nm at $f = 1$ Hz. The peak temperature of χ" is evaluated as a magnetic blocking temperature T_{B}. At $f = 1$ Hz, T_{B} hardly changes at P of 2.7 kbar, and it prominently shifts for $P \geq 6.2$ kbar. The frequency dependence of the inverse of T_{B} under pressure is shown against $\ln(2\pi f)$ in Fig. 3(b). The linear manner

in the so-called Arrhenius plot is reproduced with

$$\frac{1}{T_{\text{B}}} = -\frac{k_{\text{B}}}{\Delta E}\ln(2\pi f) + \ln(\tau_0)$$ (1)

where $\Delta E/k_{\text{B}}$ is an activation energy, k_{B} is the Boltzmann constant, and τ_0 is a pre-factor. Figure 3(c) shows the pressure dependence of $\Delta E/k_{\text{B}}$: $\Delta E/k_{\text{B}}$ exhibits the maximum at 3.5 $\pm$ 1.0 kbar. ΔE is proportional to effective magnetic anisotropy.

Figures 4(a) and 4(b) show the magnetization curve (a) and the pressure dependence of the coercive field H_{c} (b). As mentioned in Section I, the magnetic property for the bulk NiO is antiferromagnetic. The magnetic hysteresis seen in (a) originates in the blocking phenomenon of the single-domain magnetic structure stabilized by the decrease in D. H_{c} exhibits a maximum at 4 ± 1 kbar, suggesting that there is a maximum in effective magnetic anisotropy there. This is consistent with the change in $\Delta E/k_{\text{B}}$, suggesting the possibility of any structural change. In the next section, we investigate the crystal structure of nanocrystalline NiO with $D = 11.4$ nm, along with the other three nanocrystalline samples.

B. Structural analysis

Figure 5 shows the XRD profiles of the rhombohedral (012) plane for the NiO nanocrystals with $D = 24.6$ (a), 17.1 (b), 11.4 (c), and 8.6 nm (d) under pressure. At first, we focus on the shift of the peak position for $D = 11.4$ nm (see Fig. 5(c)). Careful observation shows that the reverse change in peak shift occurs at $P = 1.6$-3.6 kbar. Similar phenomena are observed at approximately $P = 9.2$ kbar for $D = 24.6$ nm and 3.6 kbar for $D = 17.1$ nm. At $D = 8.6$ nm, diffraction peaks monotonously shift toward the higher angle side. Figures 6, 7, 8, and 9 show the pressure dependence of structural parameters estimated in the hexagonal unit cell based on the rhombohedral system for $D = 24.6$, 17.1, 11.4, and 8.6 nm, respectively. The results on the unit cell volume V are of direct help for imaging whether the unit cell expands or shrinks under pressures. Herein, we define the characteristic pressure P_{c} where V exhibits a temporal increase.

As shown in Fig. 6(b), for $D = 24.6$ nm, the unit cell volume V exhibits a small increase at around $P = 7$ kbar within the decreasing trend. The increase in c/a with a magnitude of more than 1 % suggests elongation along the [111] direction of the fcc cell. As seen in Fig. 6(a), c tends to increase, while a decreases. The small increase in V originates in the

7

down-and-up in c at $P = P_{\rm c}$.

For $D = 17.1$ nm, both a and c have a maximum at approximately $P = 4$ kbar (Fig. 7(a)), so that V exhibits prominent maximum at $P = P_{\rm c}$ (Fig. 7(b)). On the other hand, c/a keeps the value of 2.449 ± 0.004 (within 0.2 % of the average) (see Fig. 7(b)).

For $D = 11.4$ nm, c decreases, while a exhibits a temporal increase below $P = 2$ kbar (see Fig. 8(a)). Both seem to be constant for $P > 10$ kbar. As seen in Fig. 8(b), V shows a similar pressure dependence to that of a, and it has a maximum at approximately $P = 2$ kbar. Below 10 kbar, the unit cell shrinks along the [111] direction of the fcc lattice.

For $D = 8.6$ nm, V decreases with increasing pressure, and there is a small change in the slope at around 5 kbar (see Fig. 9(b)). There a has a maximum, while c has a minimum (see Fig. 9(a)). c/a has a minimum at this pressure. Nevertheless, V continues to exhibit monotonous decrease, and it does not exhibit a remarkable change in the pressure region up to more than 20 kbar.

It is stressed that the manner of structural change in the unit cell level depends on the crystalline size. The mechanism of the V expansion also depends on the crystalline size. Figure 10 shows the D dependence of the characteristic pressure $P_{\rm c}$ for the temporal expansion in the unit-cell volume. In the D region covered by the experiments of nanocrystals, $P_{\rm c}$ decreases with decreasing D as $P_{\rm c}$ [kbar] $= 0.43 \times D$ [nm] - 3.43. The pressure value produced by DAC increases with decreasing temperature [27]. In each nanocrystal, anomalous structure-change at liquid helium temperature will appear above $P_{\rm c}$ estimated by the XRD analysis at room temperature.

IV. EXPERIMENTAL RESULTS OF BULK NIO ∼ ABOUT VOLUME EXPANSION ∼

We confirm whether the characteristic expansion of the unit cell at low pressure, observed in nanocrystals with $D \geq 11.4$ nm, would occur in bulk crystal or not. Here, we prepare three kinds of situations: (1) an experiment for quasi-hydrostatic (anisotropic) compression, (2) an experiment for good hydrostatic (quite isotropic) compression, and (3) a DFT calculation for ideal hydrostatic (perfectly isotropic) compression.

(1) Quasi-hydrostatic compression. We observed the change in the XRD profile of the rhombohedral (012) plane at pressures up to $P = 31$ kbar in the case of using a transport

fluorinated FC77 as PTM. The behavior of bulk NiO observed there is similar to that for the NiO nanocrystals with $D = 24.6$ nm. It is known that FC77 solidifies below 1 GPa at room temperature [28], similar to the Apiezon-J oil used in the magnetic measurements. When being pressurized at room temperature, isotropic compression is not guaranteed (*i.e.* anisotropic compression is imaged in Fig. 2(b)). Below 5 kbar, its diffraction peak shifts toward higher angle sides, whereas at approximately 5 kbar, the change in its peak reverses. Above 7 kbar, it again exhibits systematical shifts toward higher angle sides. The structural parameters of the hexagonal unit cell estimated on the basis of the rhombohedral system are shown as a function of P in Fig. 11(a)-(d), along with the results of the other two situations. For $P < 6$ kbar, the structural parameters a, c, and V decrease with increasing P, whereas at approximately $P = 7$ kbar, all of them exhibit prominent jump. a/c only exhibits the stagnation in its decreases with increasing P at around $P = 4$–7 kbar.

(2) Good hydrostatic compression. PTM is changed to a mixture of methanol and ethanol with the ratio of 4:1 (abbreviated as ME) that maintains a liquid state in the considered pressure region [29]. There it is expected that good hydrostatic compression close to an ideal case could be realized. There is no anomalous expansion of the unit cell, and c/a hardly changes with compression.

(3) Ideal hydrostatic compression. As for ideal hydrostatic compression, the DFT calculation is conducted. All of a, c, and V decrease linearly against pressure, and a/c keeps a constant. They reproduce the trend of the change in lattice parameters observed in (2). Thus it is noted that the unit cell expansion observed experimentally originates in anisotropic compression maybe due to the change in viscosity or the solidification of PTM.

V. DISCUSSION

The pressure effects on bulk NiO had been investigated in terms of the magneto-structural correlation by many scientists. The pressure region exceeded 100 GPa [30–32], and the pressure transmitting medium (PTM) has variety including being not used. Indeed, their interests have been paid to more than 10 GPa as presented in the maximum pressure of 8 GPa (NaCl as PTM) [33], 9 GPa (4:1 ethanol-methanol mixture) [34], 30 GPa [35], 67 GPa (tungsten powders) [36], 141 GPa (4:1 ME) [30], and 280 GPa [31]. Recently the insulator-metal transition in highly-compressed NiO without PTM was observed at 240 GPa [32]. We

stress that the structural change at pressures of below 1 GPa has never been investigated in detail.

The preliminary DFT calculation for pressures of up to 50 GPa suggests that the rhombohedral structure remains stable even for $P \leq 50$ GPa. The aforementioned temporal expansion of the unit cell cannot be concluded as a simple structural change like the transition from cubic to rhombohedral. Anomalous unit-cell expansion should be discussed in the frame of rhombohedral unit cells. It becomes unstable with decreasing the crystalline size as shown in Fig. 10, and it vanishes at approximately 8 nm. It is imaged by watching the change in the lattice parameters in the unit cell. For instance, in $D = 8.6$ nm for $P < 10$ kbar, large contraction along the c-axis overcomes small elongation along the a-axis, whereas for $P > 10$ kbar, contraction along the a-axis under keeping c constant determines the decrease in V. An aspect of temporal unit-cell expansion for $D = 11.4$ nm was also observed via the magnetic measurements, suggesting that it brings about the change in magneto-crystalline anisotropy.

It had been known that the nanocrystalline NiO has a multi-sublattice different from a two-sublattice, resulting in the appearance of large magnetic moments [13]. In the NiO nanocrystals synthesized in mesoporous silica, at around 3 nm, the rhombohedral structure of the nanocrystals is severely strained, and the unit cell volume has the maximum value [15]. There the magnetic anisotropy is greatest, suggesting the remarkable magneto-structural correlation.

It is stressed that the spin system is strongly coupled with the crystal structure. The change in magnetic properties such as ΔE and H_c is more prominent than that in the crystal structure. Effective magnetic anisotropy can become a window to observe the anomalous unit-cell expansion. The detailed mechanism is not clear. We suppose that the spin-orbit interaction might bring about the strong magneto-structural correlation.

Some of us had investigated anisotropic compression effects on $LaMnO_{3+\delta}$ nanocrystals synthesized in SBA-15 [16]. The nanocrystals with $D \sim 10$ nm consist of ferromagnetic and antiferromagnetic particles. The structural system of $LaMnO_{3+\delta}$ is a rhombohedral structure as well. The lattice constants were found to reduce anisotropically, and the values saturated above a critical pressure. The magnitude of the change in c/a is comparable with those observed in the present NiO nanocrystals. Both the ferromagnetic and antiferromagnetic transition temperatures initially increased with increasing pressure and then remained

constant at around the critical pressure. The change in those transition temperature is approximately 10 K. In previous literature, anisotropic stress was related with distortion of the shape of the nanocrystals, which induces an increase in the lattice strain and the anisotropic compression of the crystal structure. Now, in NiO, through the prominent unit-cell expansion induced with anisotropic compression, we can modify the magnetic anisotropy of magnetic nanocrystals.

Recently we have observed similar anomalous deformation in the unit cell in a superconductor [17]. In severely strained Nb under non-hydrostatic compression using such PTM as FC77, bcc structure brings about non-isotropic deformation: In a pressure region, unit cell volume hardly changes. At least along a direction, the lattice constant increases. This experiment has a starting material that has heavy strain. The artificial compression by pressure apparatus has more accumulated residual strain. However, the unit cell with high symmetry cannot accumulate large strain forever. At a characteristic pressure, P_c, the strain is released, so that structural symmetry is lowered. The above structural change might be seen often in the unit cell structure with high symmetry. In the case of NiO, the decrease in D brings about the decrease in the capacity of accumulating strain, resulting in the decrease in P_c. Fortunately, nanocrystalline NiO has ferromagnetic moments, and the release of accumulated strain can be observed via magnetic measurements.

VI. CONCLUSION

NiO has strong magneto-structural correlation that induces ferromagnetic moments in nano-sized crystals. The nanocrystalline NiO with $D = 11.4$ nm, synthesized in one-dimensional pores, was compressed without stress in a direction parallel to the silica walls. At low pressures, the magnetic blocking phenomenon peculiar to the single-domain magnet is strengthened, and the coercive field in the magnetization curve is also enhanced. These behaviors are related to the unit-cell expansion. Thus, the magnetic anisotropy of nano-sized crystals can be modified by external stress. As a candidate, the enhancement of spin-orbital interactions may trigger the increase in the magnetic anisotropy. Temporal unit-cell expansion originates in non-hydrostatic compression, and indeed the bulk crystal also exhibits similar change at around 7 kbar under similar circumstances. As the crystalline size decreases, the characteristic pressure for negative compression decreases, and the anomalous

negative contraction vanishes at approximately 8 nm. Thus, by utilizing unit-cell expansion, we can increase the magnetic anisotropy of nanocrystalline NiO artificially.

Acknowledgments

---

[1] W. L. Roth, Phys. Rev. **110**, 1333 (1958).

[2] D. S. Rodbell and J. Owen, J. Appl. Phys. **35**, 1002 (1964).

[3] B. Morosin, Phys. Rev. B **1**, 236 (1970).

[4] K. Terakura, A. R. Williams, T. Oguchi, and J. Kübler, Phys. Rev. Lett. **52**, 1830 (1984).

[5] K. Terakura, T. Oguchi, A. R. Williams, and J. Kübler, Phys. Rev. B **30**, 4734 (1984).

[6] G. A. Sawatzky and J. W. Allen, Phys. Rev. B **53**, 2339 (1984).

[7] J. M. McKay and V. E. Henrich, Phys. Rev. Lett. **53**, 2343 (1984).

[8] G. A. Sawatzky and J. W. Allen, Phys. Rev. Lett. **53**, 2339 (1984).

[9] M. R. Norman and A. J. Freeman, Phys. Rev. B **33**, 8896 (1986).

[10] M. D. Towler, N. L. Allan, N. M. Harrison, V. R. Saunders, W. C. Mackrodt, and E. Apra, Phys. Rev. B **50**, 5041 (1994).

[11] S. L. Dudarev, L.-M. Peng, S. Y. Savrasov, and J.-M. Zuo, Phys. Rev. B **61**, 2506 (2000).

[12] C. Rödl, F. Fuchs, J. Furthmüller, and F. Bechstedt, Phys. Rev. B **79**, 235114 (2009).

[13] R. H. Kodama, S. A. Makhlouf, and A. E. Berkowitz, Phys. Rev. Lett. **79**, 1393 (1997).

[14] S. A. Makhlouf, H. Al-Attar, and R. H. Kodama, Solid State Commun. **145**, 13 (2008).

[15] T. Tajiri, S. Saisho, M. Mito, H. Deguchi, K. Konishi, and A. Kohno, J. Phys. Chem. C **119**, 1194 (2015).

[16] T. Tajiri, S. Saisho, Y. Komorida, M. Mito, H. Deguchi, and A. Kohno, J. Appl. Phys. **110**, 044307 (2011).

[17] M. Mito, Y. Kitamura, T. Tajiri, K. Nakamura, R. Shiraishi, K. Ogata, H. Deguchi, T. Yamaguchi, N. Takeshita, T. Nishizaki, et al., J. Appl. Phys. **125**, 125901 (2019).

[18] M. Mito, J. Phys. Soc. Jpn. Suppl. A **76**, 182 (2007).

[19] A. Fujiwara, K. Ishii, T. Watanuki, H. Suematsu, H. Nakao, K. Ohwada, Y. Fujii, Y. Murakami, T. Mori, H. Kawada, et al., J. Appl. Cryst. **33**, 1241 (2000).

[20] G. J. Piermarini, S. Block, J. D. Barnett, and R. A. Forman, J. Appl. Phys. **46**, 2774 (1975).

[21] F. Izumi and K. Momma, Solid State Phenom. **130**, 15 (2007).

[22] J. Yamauchi, M. Tsukada, S. Watanabe, and O. Sugino, Phys. Rev. B **54**, 5586 (1996).

[23] D. Vanderbilt, Phys. Rev. B **41**, 7892 (1990).

[24] K. Laasonen, A. Pasquarello, R. Car, C. Lee, and D. Vanderbilt, Phys. Rev. B **47**, 10142 (1993).

[25] J. P. Perdew, K. Burke, and M. Ernzerhof, Phys. Rev. Lett. **77**, 3865 (1996).

[26] M. Bernasconi, G. L. Chiarotti, P. Focher, S. Scandolo, E. Tosatti, and M. Parrinello, J. Phys. Chem. Solid **56**, 501 (1995).

[27] M. Mito, M. Hitaka, T. Kawae, K. Takeda, T. Kitai, and N. Toyoshima, Jpn. J. Appl. Phys. **40**, 6641 (2001).

[28] T. Varga, A. P. Wilkinson, and R. J. Angel, Rev. Sci. Instrum. **74**, 4564 (2003).

[29] I. Fujishiro, G. J. Piermarini, S. Block, and R. G. Munro, in *High Pressure in Research and Industry, Proceedings of the 8th AIRAPT Conference* Vol.II (p. 608) (edited by C. M. Backman, T. Johannisson and L. Tegner, Arkitektkopia, Uppsala, Sweden, 1982).

[30] T. Eto, S. Endo, M. Imai, Y. Katayama, and T. Kikegawa, Phys. Rev. B **61**, 14984 (2000).

[31] V. Potapkin, L. Dubrovinsky, I. Sergueev, M. Ekholm, I. Kantor, D. Bessas, E. Bykova, V. Prakapenka, R. P. Hermann, R. RNuffer, et al., Phys. Rev. B **93**, 201110 (2016).

[32] A. G. Gavriliuk, I. A. Trojan, and V. V. Struzhkin, Phys. Rev. Lett. **109**, 086402 (2012).

[33] I. Wakabayashi, H. Kobayashi, H. Nagasaki, and S. Minomura, J. Phys. Soc. Jpn. **25**, 227 (1968).

[34] A. G. Gavrilyuk, I. A. Troyan, I. S. Lyubutin, and V. A. Sidorov, Sov. Phys. JETP **92**, 696 (2001).

[35] R. L. Clendenen and H. G. Drickamer, J. Chem. Phys. **44**, 4223 (1966).

[36] L. Liu, X. D. Li, J. Liu, S. Jiang, Y. C. Li, G. Y. Shen, H. K. Mao, Y. Bi, and J. Xu, J. Appl. Phys. **104**, 113521 (2008).
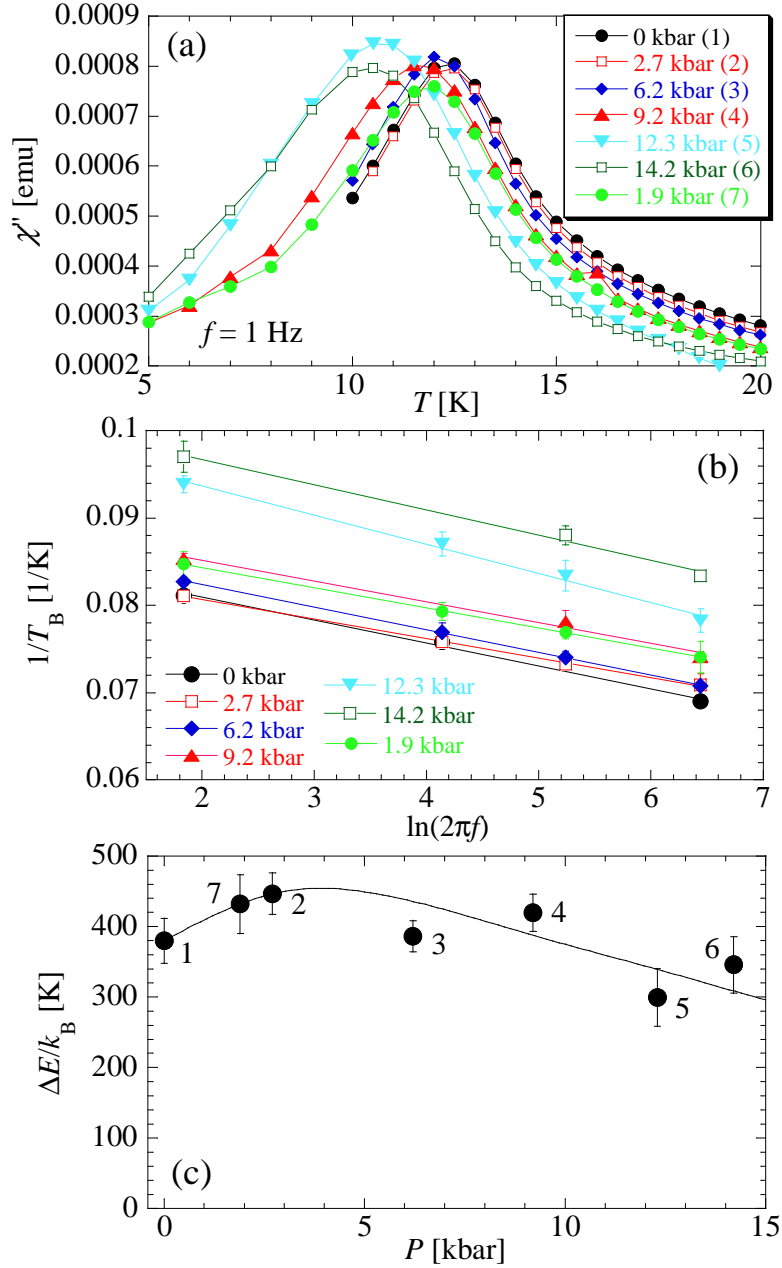
FIG. 3: (a) Out-of phase of ac magnetic susceptibilities χ'' of nanocrystalline NiO with $D = 11.4$ nm, (b) Arrhenius plot exhibiting the pressure change in the frequency dependence of the blocking temperature T_B, and (c) pressure dependence of activation energy E/k_B. In (a), the magnitude of χ'' is normalized with the mass of the sample consisting of SBA-15 and NiO. The number beside each pressure value in (a) and that beside each symbol in (c) indicate the measurement trial number. The solid curves in (a) and (c) are guides for the eyes, and the solid lines in (b) express Eq. (1).

14
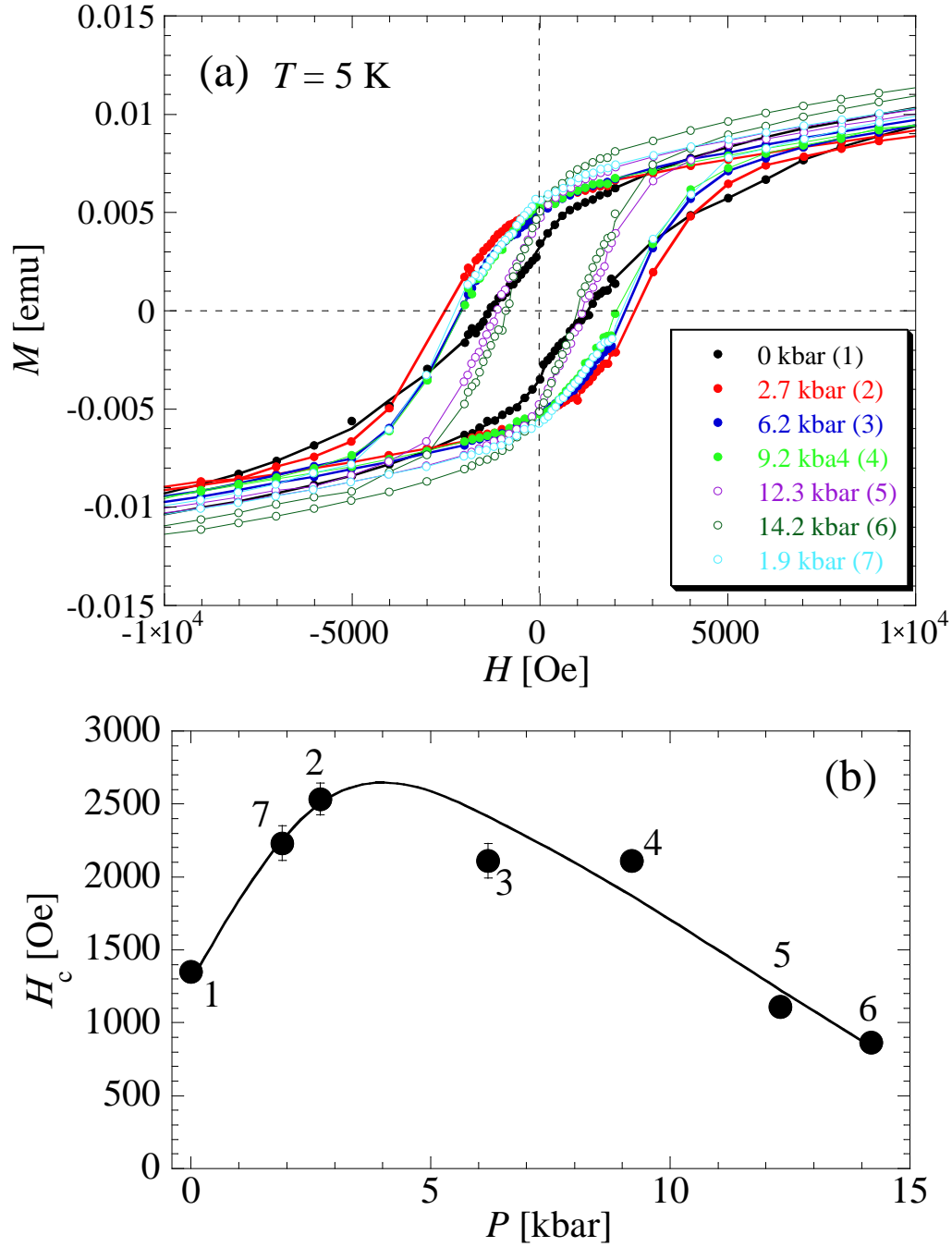
FIG. 4: (a) Magnetization hysteresis for nanocrystalline NiO with $D = 11.4$ nm at several pressures up to 14.2 kbar. The magnetic field H was scanned as 50 kOe $\rightarrow$ -50 kOe $\rightarrow$ 50 kOe at $T = 5$ K. (b) Pressure dependence of the magnetization coercive field H_c at $T = 5$ K. The number beside each pressure value in (a) and that beside each symbol in (b) stand for the order in which the measurements were taken.
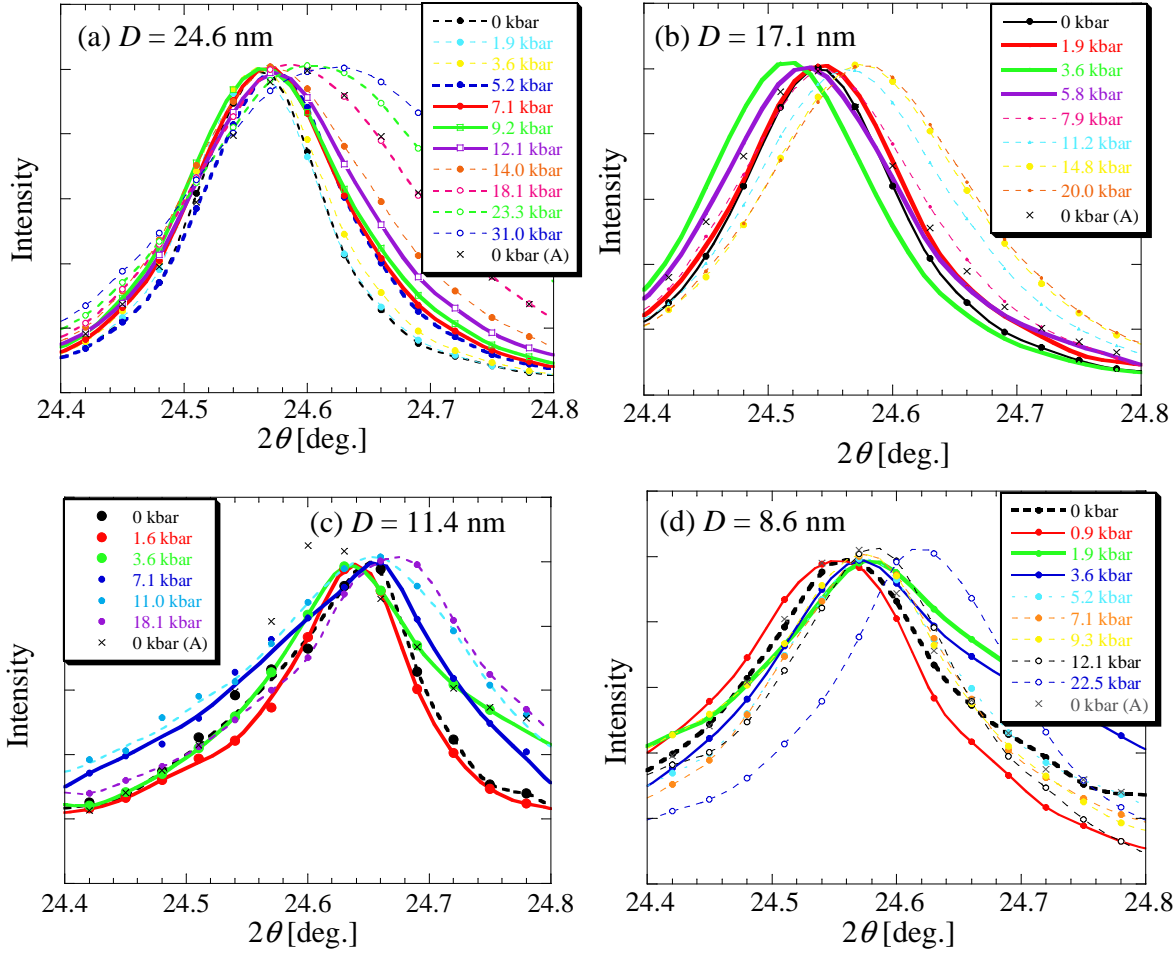
FIG. 5: XRD profile of the rhombohedral (012) plane of nanocrystalline NiO with $D = 24.6$ (a), 17.1 (b), 11.4 (c), and 8.6 nm (d) under pressure. Only the profiles at around the characteristic pressure P_c are shown with the solid curves (the others are broken curves). The pressure value was increased gradually up to the maximum. The expression of 0 kbar (A) represents the data at ambient pressure after releasing the maximum pressure.
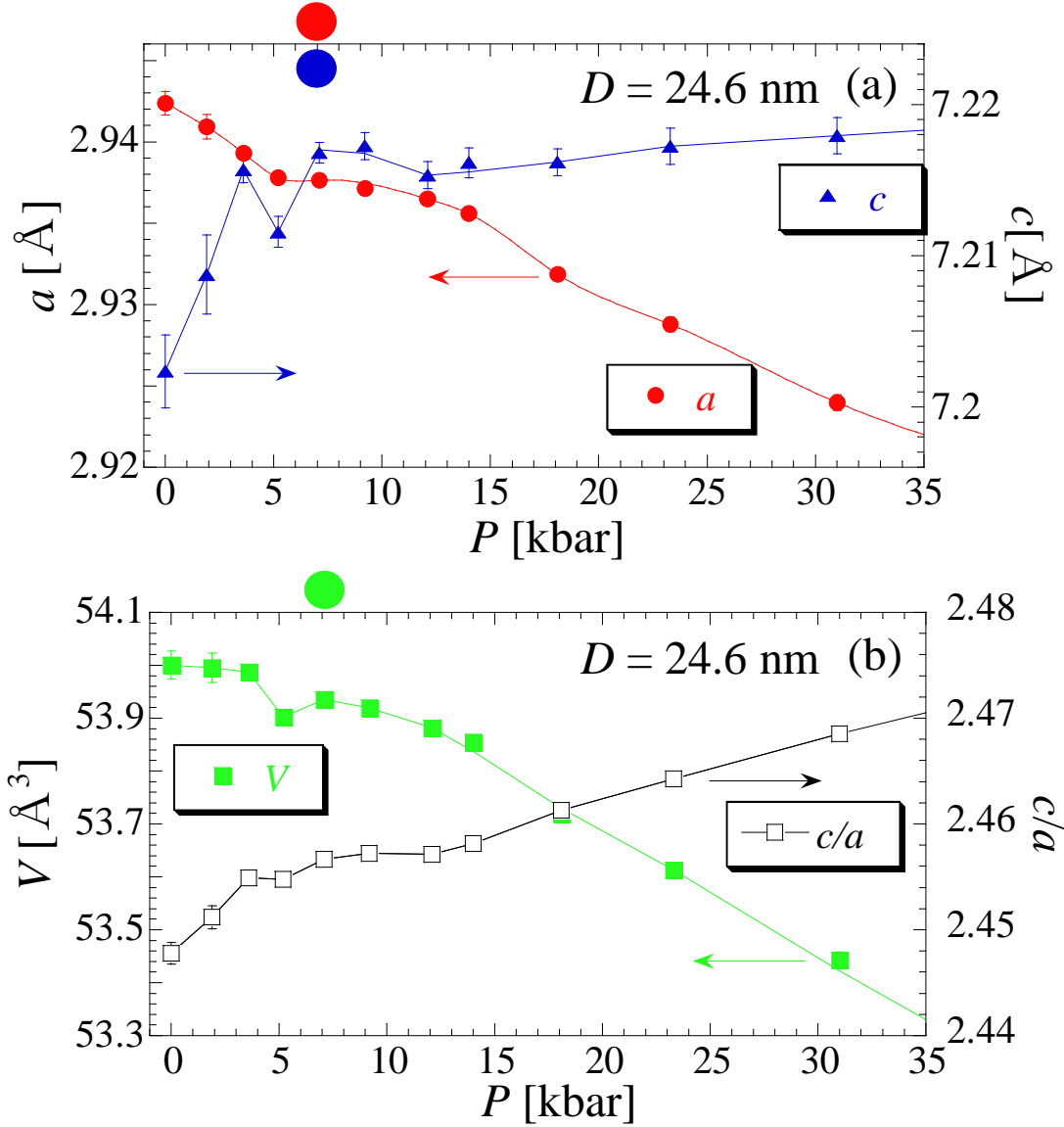
FIG. 6: Pressure dependence of structural parameters such (a) lattice parameters a (red circle) and c (blue triangle) and (b) unit cell volume V (green square) and c/a (black hollow square) under the rhombohedral structure for the NiO nanocrystals with $D = 24.6$ nm. For all data, error bars are attached, whereas they are too small to visible. For each parameter, the characteristic pressure related to anomalous lattice expansion is marked by a closed circle with the corresponding color.
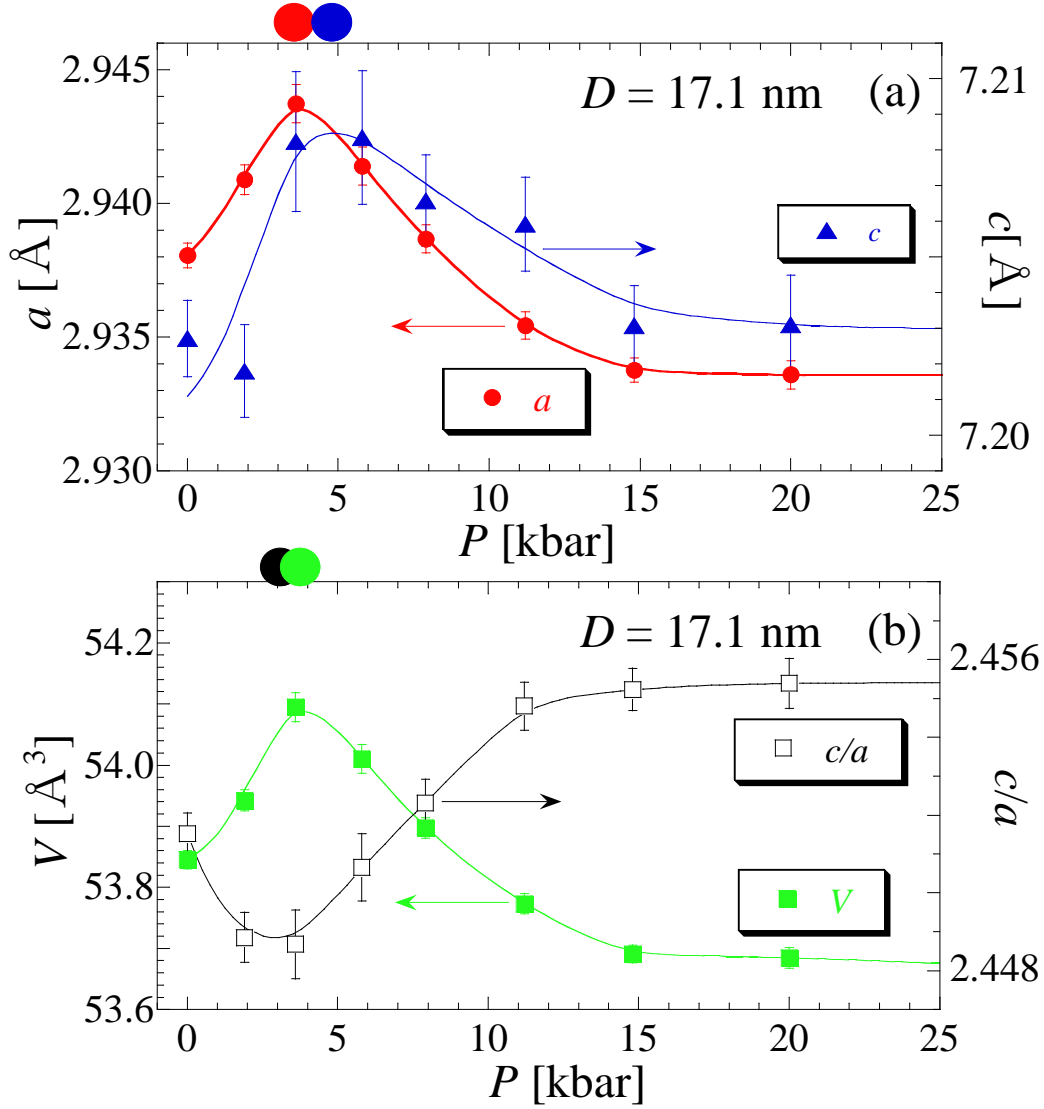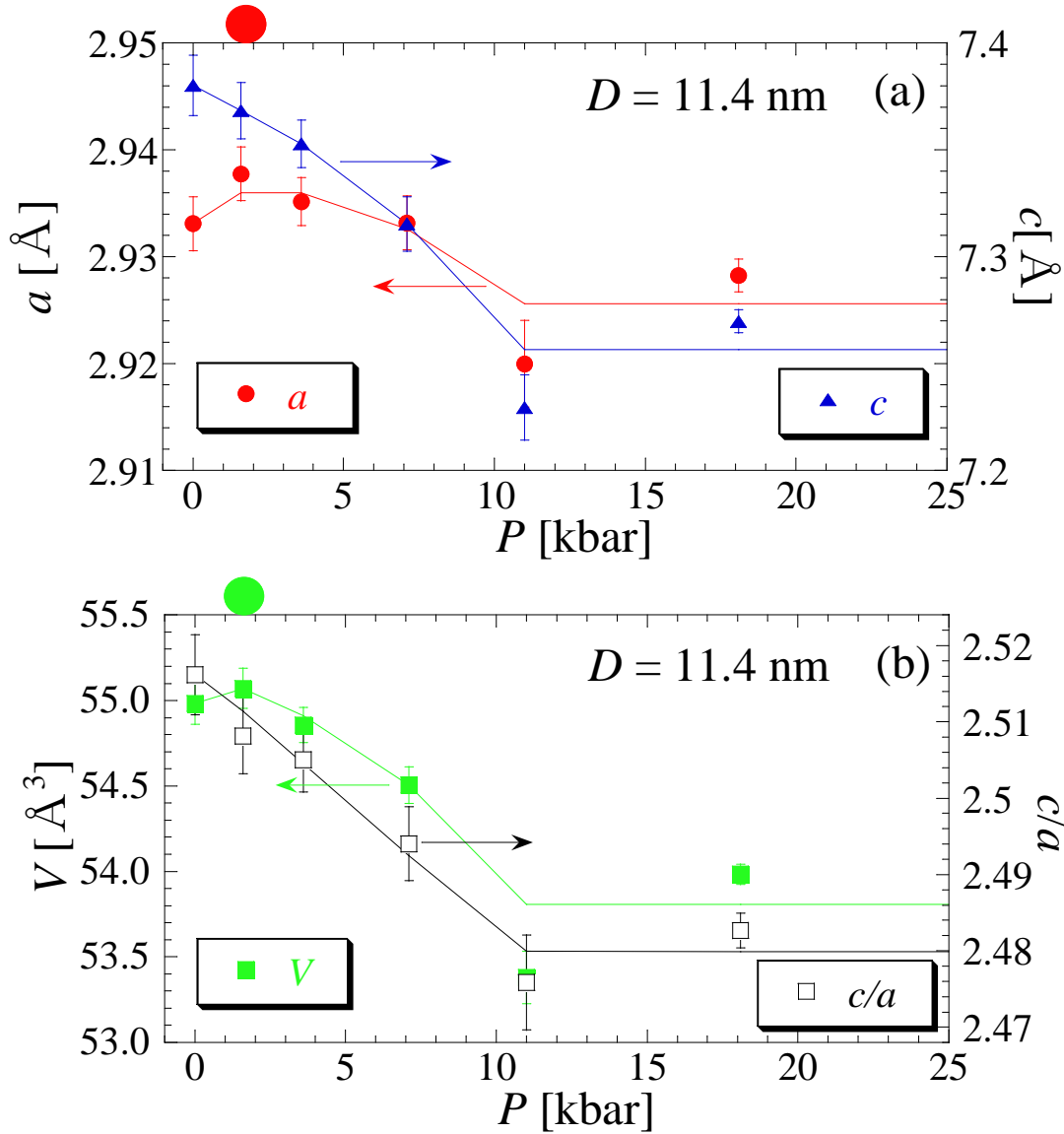
FIG. 7: Pressure dependence of structural parameters such (a) lattice parameters such (a) lattice parameters a (red circle) and c (blue triangle) and (b) unit cell volume V (green square) and c/a (black hollow square) under the rhombohedral structure for the NiO nanocrystals with $D = 17.1$ nm. For each parameter, the characteristic pressure related to anomalous lattice expansion is marked by a closed circle with the corresponding color.

FIG. 8: Pressure dependence of structural parameters such (a) lattice parameters such (a) lattice parameters a (red circle) and c (blue triangle) and (b) unit cell volume V (green square) and c/a (black hollow square) under the rhombohedral structure for the NiO nanocrystals with $D = 11.4$ nm. For each parameter, the characteristic pressure related to anomalous lattice expansion is marked by a closed circle with the corresponding color.
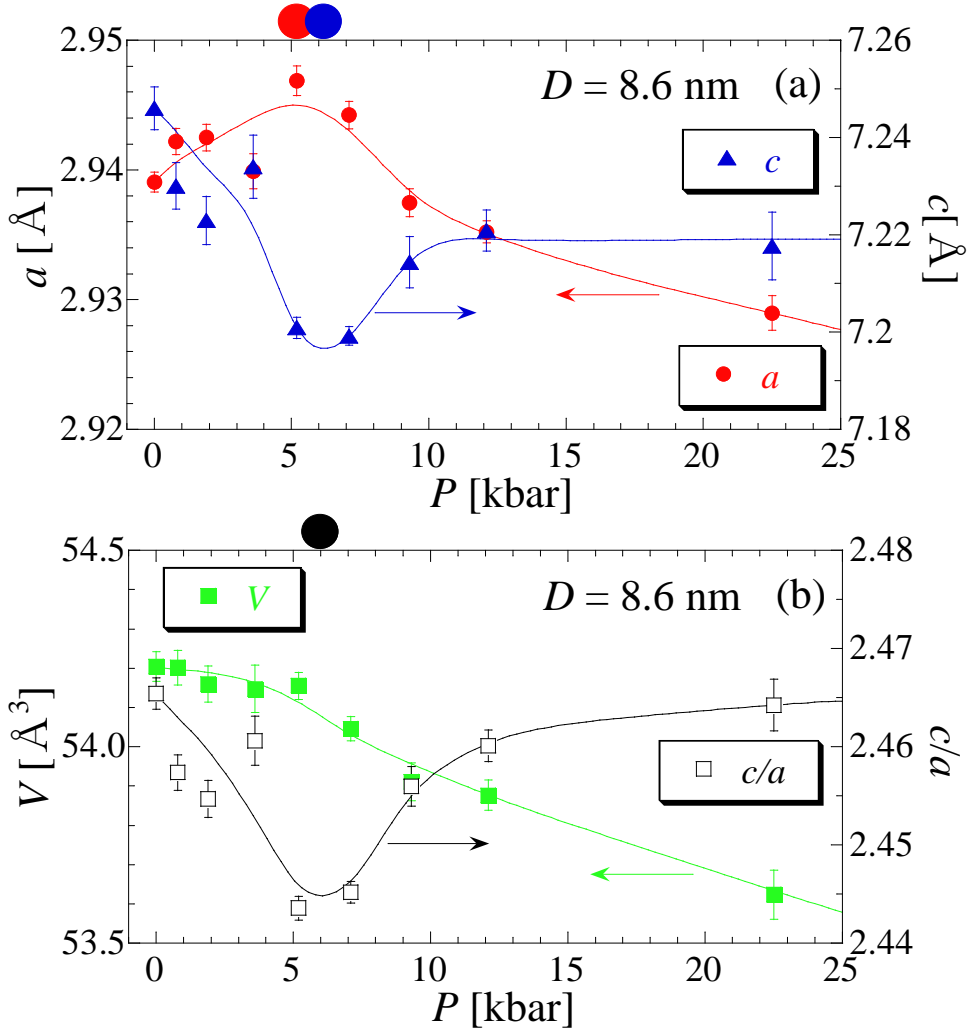
19

FIG. 9: Pressure dependence of structural parameters such (a) lattice parameters such (a) lattice parameters a (red circle) and c (blue triangle) and (b) unit cell volume V (green square) and c/a (black hollow square) under the rhombohedral structure for the NiO nanocrystals with $D = 8.6$ nm. For each parameter, the characteristic pressure related to anomalous lattice expansion is marked by a closed circle with the corresponding color.
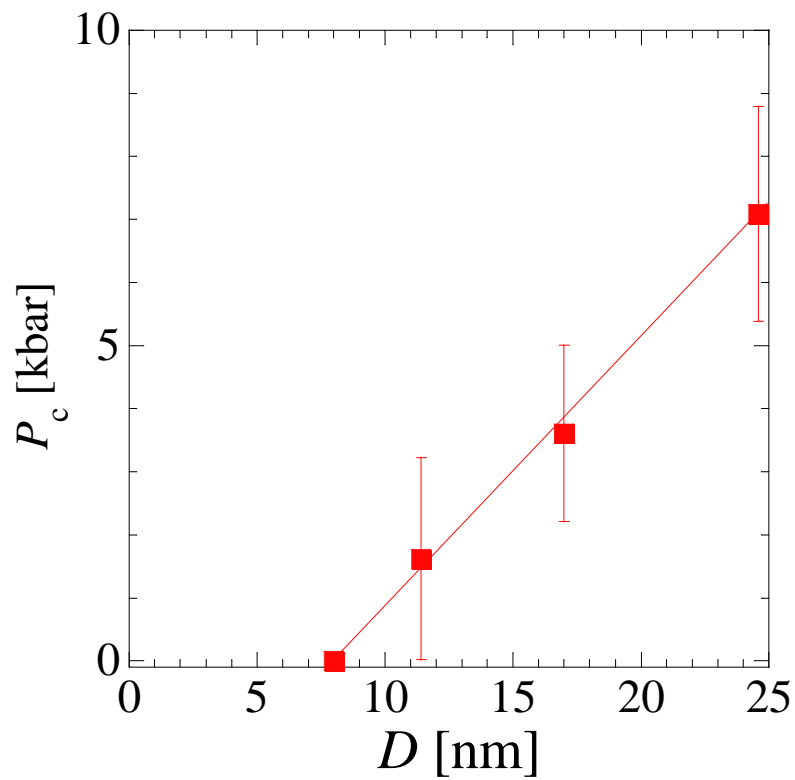
FIG. 10: Crystalline size dependence of P_c that is a characteristic pressure for temporary volume expansion of the unit cell. The solid lines for ≥ 7 kbar stands for P_c [kbar] $= 0.43 \times D$ [nm] - 3.43.
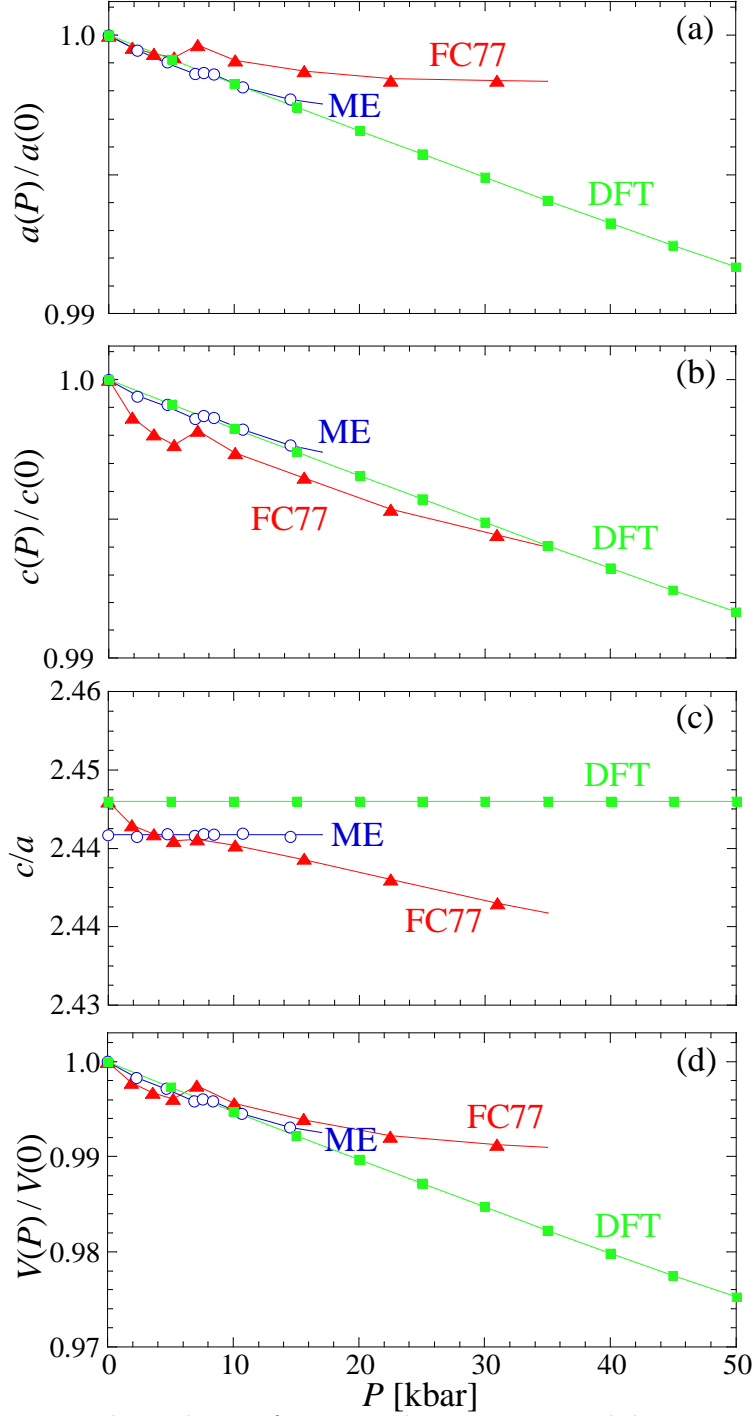
FIG. 11: Pressure dependence of structural parameters such lattice parameters a (a), c (b), c/a (c), and unit cell volume V (d) under considering the hexagonal structure based on the rhombohedral structure in the case of using FC77 and ME as PTM. For reference, we also plot the DFT calculation results assuming ideally isotropic compression. The lattice parameters under pressure such as $a(P)$, $c(P)$, and $V(P)$ are normalized with those values at $P = 0$, respectively. In the DFT calculation, a/c keeps a constant.